



# Five-parameter grain boundary characterisation of randomly textured AZ31 Mg alloy

Hossein Beladi<sup>a</sup>, Alireza Ghaderi<sup>a</sup> and Gregory S. Rohrer<sup>b</sup>

<sup>a</sup>Institute for Frontier Materials, Deakin University, Geelong, Australia; <sup>b</sup>Department of Materials Science and Engineering, Carnegie Mellon University, Pittsburgh, PA, USA

## ABSTRACT

The five-parameter analysis approach was used to measure the grain boundary character distribution of randomly textured AZ31 Mg alloy produced through casting followed by annealing at 450°C for 16 h. The misorientation angle distribution was close to the one expected from the material with a random texture. The grain boundary plane distribution, ignoring the misorientation angle, revealed a relatively weak plane orientation anisotropy, with a preference for grain boundaries terminated on prismatic  $\{hki0\}$  planes. Surprisingly, the population of grain boundary planes was not inversely related to the expected grain boundary energies. Basal oriented grain boundaries are expected to have the lowest energy, but they also had the lowest population. This could result from the presence of residual columnar grains, formed during solidification and remaining after annealing, which increases the relative area of boundary planes with prismatic orientations.

## ARTICLE HISTORY

Received 15 July 2019  
Accepted 29 October 2019

## KEYWORDS

AZ31; grain boundary;  
random texture; EBSD

## Introduction

Magnesium alloys have received increased attention among different industries (e.g. automotive and electronics) because of their moderate strength along with low density. However, they mostly suffer from low ductility at room temperature due to the restricted activation of slip systems (i.e. non-basal slip) [1,2]. Instead, deformation twinning is the commonly observed deformation mode in Mg alloys [2]. The deformation twins largely nucleate at grain boundaries, as stress is concentrated in the vicinity of grain boundaries to maintain compatibility during the straining [3]. Therefore, the grain boundary area is believed to affect the deformation twin density, though the grain size limits the twin growth [4]. However, it was recently demonstrated that the propensity for deformation twinning nucleation is not similar for all grain boundaries [3]. This suggests that the grain boundary characteristics, to some extent, affect the deformation twinning nucleation and this motivates a study of the distribution of

**CONTACT** Hossein Beladi  [hossein.beladi@deakin.edu.au](mailto:hossein.beladi@deakin.edu.au)  Institute for Frontier Materials, Deakin University, Geelong, VIC 3216, Australia

© 2019 Informa UK Limited, trading as Taylor & Francis Group

grain boundaries according to their crystallographic character, including misorientation and grain boundary plane.

The grain boundary is a three-dimensional microstructural feature characterised by five independent crystallographic parameters. Three parameters define the lattice misorientation (i.e. three Euler angles) and two parameters define the plane normal [5]. Therefore, special approaches such as transmission electron microscopy [6] and three-dimensional electron back-scattered diffraction (3D-EBSD) [7,8] techniques are required to fully characterise grain boundaries in polycrystalline materials. Recently, a stereological method was developed to determine the grain boundary plane distribution from conventional two-dimensional EBSD data [9]. This technique has been frequently employed to study grain boundary plane distributions in a variety of polycrystalline materials [10–13]. The main aim of the current study was to provide a comprehensive description of the grain boundary character distribution of a cast and annealed AZ31 Mg alloy with a random texture using the five-parameter grain boundary analysis technique from two-dimensional EBSD data.

## Experimental procedure

An as-cast material was made through remelting an AZ31 magnesium alloy (Mg–3%Al–1%Zn, in wt%) ingot at 800°C in a stainless steel crucible under inert gas. The melt was poured at ~ 720°C in a chill mould to solidify under inert gas. The employment of a chill mould was to minimise the formation of columnar (dendrite) grains during solidification, which tends to grow along  $\langle 11\bar{2}0 \rangle$  direction [14]. Afterwards, the as-cast material was reheated to 450°C and annealed for 16 h in Ar gas, followed by furnace cooling. This process made it possible to eliminate the mechanical twins formed by contraction/shrinkage during the solidification process.

The samples for electron backscatter diffraction (EBSD) were prepared using standard mechanical polishing followed by a colloidal silica slurry polish. The samples were handled carefully to minimise the formation of mechanical twins. The EBSD study was conducted using a field emission gun Quanta 3-D FEI scanning electron microscope, which was equipped with a fully automated EBSD device attachment, operated at 20 kV and 4 nA. EBSD data acquisition and post-processing were carried out using TexSEM Laboratories, Inc. software (TSL). Multiple EBSD maps were acquired, covering a total area of 1260 mm<sup>2</sup>, using a spatial step size of 5 μm on a hexagonal grid. The average confidence index was 0.56. A routine cleaning procedure, as discussed elsewhere [12], was performed on EBSD maps to extract the grain boundary segments/traces. In total, more than 226,000 grain boundary line segments, equivalent to the total boundary length of ~11,820,000 μm, were collected from all EBSD maps. The number of segments measured in the current study was above the minimum requirement for hexagonal crystals (i.e. 200,000 grain boundary

segments [5]). The grain boundary plane distribution was measured with a resolution of  $\sim 10^\circ$  using a stereological procedure, as discussed elsewhere [5]. In brief, each grain boundary line segment must be orthogonal to the boundary plane normal. Hence, all possible plane normals lie on a great circle for a given boundary line segment, which is perpendicular to the line segment on a stereographic projection. The examination of all grain boundary segments with a fixed lattice misorientation in the microstructure leads to a distribution of possible grain boundary normals. The preferred plane/s appears as a maximum in the distribution [5,9].

## Results and discussion

The as-cast microstructure consisted of coarse equiaxed and elongated (columnar) grains (see Figure 1(a)). Many of the elongated grains had orientations with respect to the section plane that are indicated by blue and green colours, corresponding to prismatic orientations. The grain grains also frequently contain twins, which formed due to the contraction/shrinkage upon solidification (shown by arrows in Figure 1(a)). The corresponding misorientation angle distribution displayed a strong peak at  $\sim 86^\circ$  misorientation, with their misorientation axis clustered about  $[11\bar{2}0]$  (Figure 1(b)). This suggests that they are largely tension twins (i.e.  $86.3^\circ/[11\bar{2}0]$ ).

After the prolonged annealing at  $450^\circ\text{C}$  for 16 h, the microstructure had coarse equiaxed grains with an average size of  $154 \pm 5 \mu\text{m}$  (Figure 2(a)). The prolonged heat treatment at  $450^\circ\text{C}$  for 16 h led to the removal of nearly all of the tension twins largely through the grain growth process, as the tension twins have high mobility [15]. The overall texture appeared relatively random with an intensity of 1.84 MRD (Figure 2(b)). The corresponding misorientation angle distribution also appeared similar to the one expected for the random

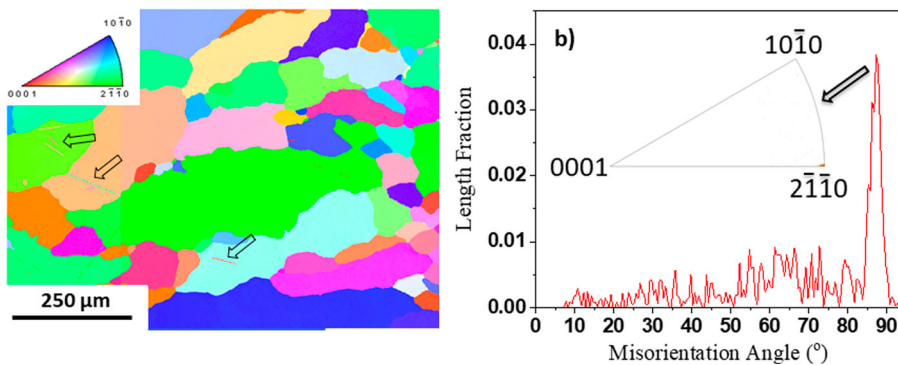


**Figure 1.** (a) EBSD image of as-cast AZ31 alloy and (b) the corresponding misorientation angle distribution along with the misorientation axis distribution at  $86 \pm 2^\circ$ . The inset in (a) represents colour codes referred to normal direction. The reader is referred to the Web version of the article for the interpretation of colours in the figure (Colour online).

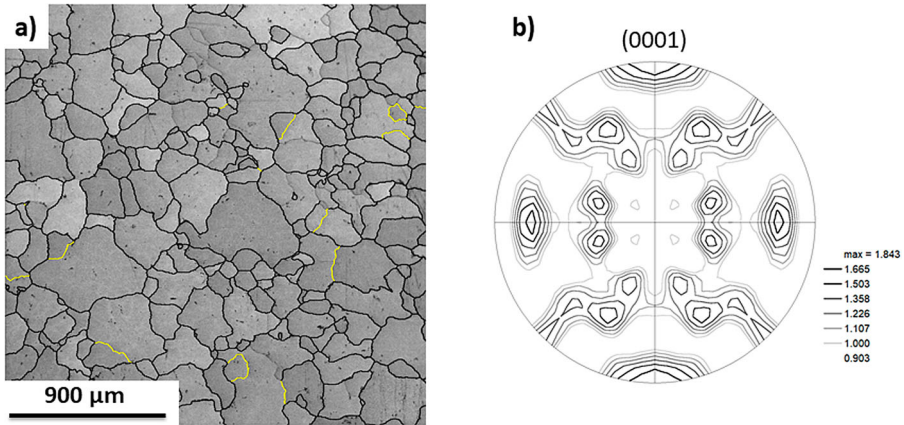


**Figure 2.** EBSD image (a) and (0001) pole figure (b) of cast AZ31 alloy followed by annealing at 450°C for 16 h. Black and yellow lines in (a) represent high angle ( $>15^\circ$ ) and  $64^\circ/[11\bar{2}0]$  grain boundaries. The reader is referred to the Web version of the article for the interpretation of colours in the figure (Colour online).

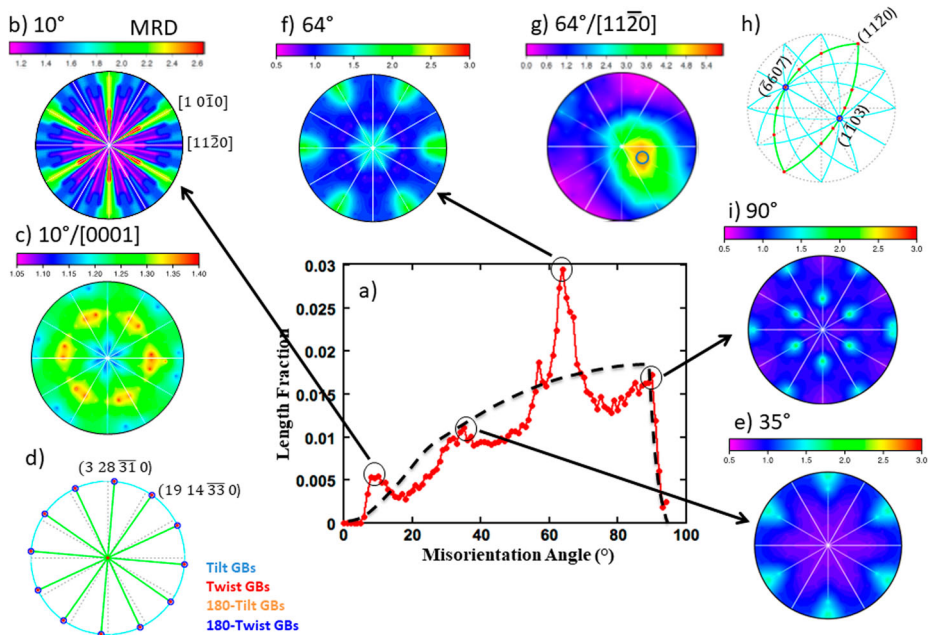


**Figure 3.** (a) The misorientation angle distribution of grain boundaries of cast AZ31 alloy followed by annealing at 450°C for 16 h. The dash black line in (a) represents the random distribution of the misorientation angle. b, e, f and i are misorientation axis distributions for  $10^\circ$ ,  $35^\circ$ ,  $64^\circ$  and  $90^\circ$  misorientation angles, respectively. The distribution of grain boundary planes character (c, g) and the corresponding calculated locations of the geometrically characteristic boundaries (d, h) [16] for lattice misorientations of  $10^\circ/[0001]$  and  $64^\circ/[11\bar{2}0]$ , respectively. Colour scale represents multiples of random distribution (MRD). The reader is referred to the Web version of the article for the interpretation of colours in the figure (Colour online).

texture, though a few peaks were still observed at misorientation angles of  $10^\circ$ ,  $35^\circ$ ,  $57^\circ$  and  $64^\circ$  (Figure 3(a)). The corresponding misorientation axis distributions at the peak positions mostly revealed maxima at the positions of  $[0001]$ ,  $\langle 10\bar{1}0 \rangle$  and/or  $\langle 11\bar{2}0 \rangle$  (Figure 3). The misorientation axis distribution at  $10^\circ$  displayed a maxima at  $[0001]$  spreading towards  $\langle 10\bar{1}0 \rangle$  (Figure 3(b)). At  $35^\circ$ , the misorientation axis distribution showed a peak at  $\langle 10\bar{1}0 \rangle$  (Figure 3 (e)). Two peaks were observed in the misorientation axis distribution for  $64^\circ$  rotations at  $[0001]$  and  $\langle 11\bar{2}0 \rangle$  (Figure 3(f)). For a  $90^\circ$  misorientation angle, the misorientation axis distribution displayed two peaks at  $\langle 11\bar{2}0 \rangle$  and  $\langle 1\bar{1}02 \rangle$  (Figure 3(i)). The distribution of grain boundary planes was plotted for the  $64^\circ/[11\bar{2}0]$  misorientation, which had the highest intensity in the axis angle

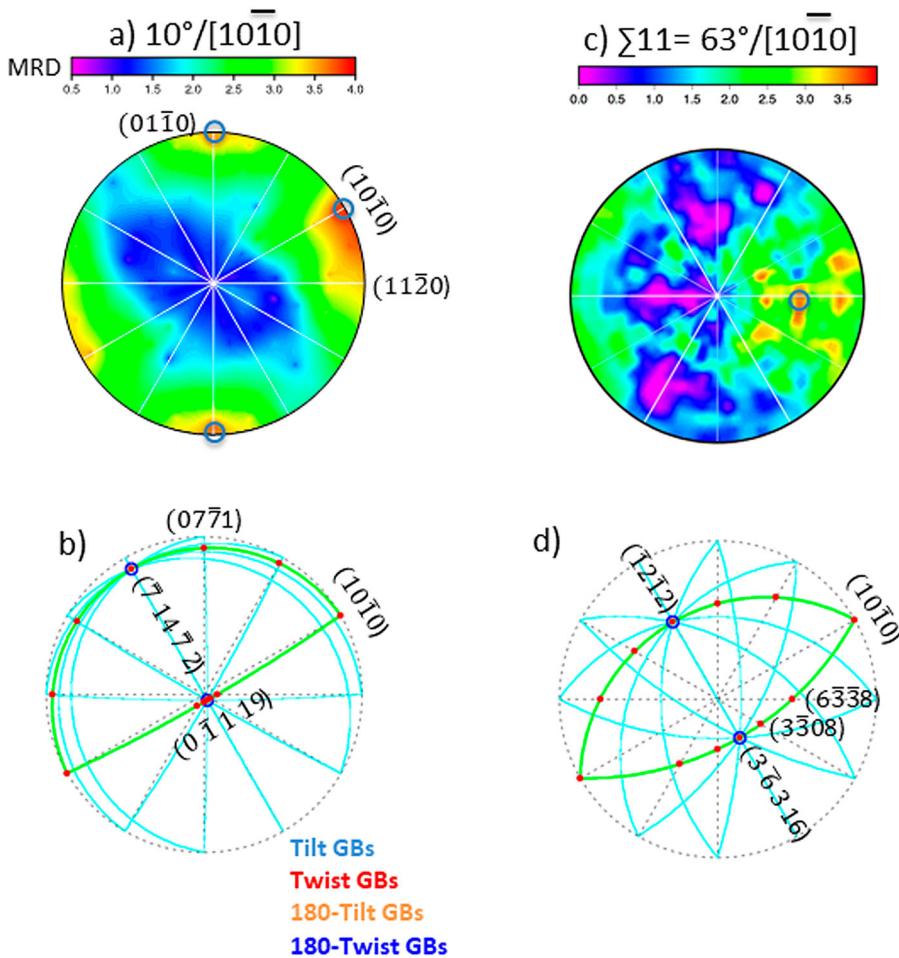


**Figure 4.** The distribution of grain boundary planes (a,c) and the corresponding calculated locations of the geometrically characteristic boundaries (b,d) [16] for different lattice misorientations: (a,b)  $10^\circ/[10\bar{1}0]$  and (c,d)  $\Sigma 11 = 63^\circ/[10\bar{1}0]$ . The open circle in a, c represent the maxima. Colour scale represents MRD. The reader is referred to the Web version of the article for the interpretation of colours in the figure (Colour online).

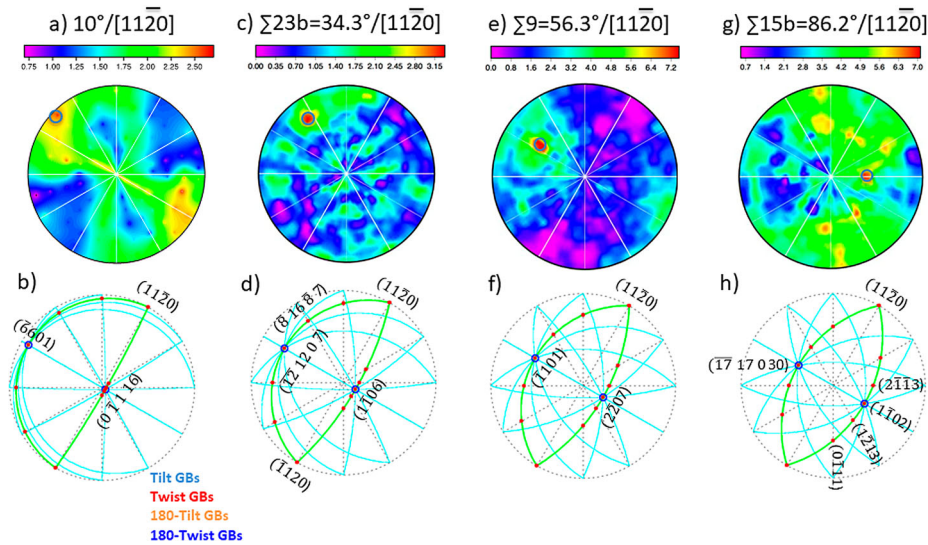


**Figure 5.** The distribution of grain boundary planes (a,c,e,g) and the corresponding calculated locations of the geometrically characteristic boundaries (b,d,f,h) [16] for different lattice misorientations: (a,b)  $10^\circ/[11\bar{2}0]$ , (c,d)  $\Sigma 23b = 34.3^\circ/[11\bar{2}0]$ , (e,f)  $\Sigma 9 = 56.3^\circ/[11\bar{2}0]$  and (g,h)  $\Sigma 15b = 86.2^\circ/[11\bar{2}0]$ . The open circle in a, c, e, g represent the maxima. Colour scale represents MRD. The reader is referred to the Web version of the article for the interpretation of colours in the figure (Colour online).

distribution, and for the  $10^\circ/[0001]$  misorientation. For each of these grain boundary plane distributions, and those presented in Figures 4 and 5, we also plot the orientations of grain boundary planes with special geometries (see Figure 3(d,h)), which include tilt, twist,  $180^\circ$ -tilt and  $180^\circ$ -twist [16]. These schematics consider all symmetries, so there can be multiple twist orientations related to equivalent representations with other misorientation axes [17]. The  $64^\circ/[11\bar{2}0]$  misorientation revealed a single peak at the position of  $(1\bar{1}04)$  orientation spreading towards  $(0001)$  orientation (i.e. along with the position of tilt boundaries), with an intensity of 6 MRD (Figure 3(g)). Within the resolution of the grain boundary plane distribution ( $10^\circ$ ) the observed maximum in the distribution at  $(1\bar{1}04)$  is consistent with the ideal position of  $180^\circ$ -twist boundary at  $(1\bar{1}03)$  (they are separated by  $10^\circ$ ). Interestingly, this is very similar to the characteristics of the compression twin. However, the compression twin is formed under a relatively large deformation [18], which is not the case here as the material subjected to the annealing treatment of  $450^\circ\text{C}$  for 16 h. The investigation of microstructure revealed that the  $64^\circ/[11\bar{2}0]$  boundaries are part of the grain boundary network formed during annealing treatment (Figure 2(a)). For the  $10^\circ/[0001]$  misorientation, the minimum appeared at  $(0001)$  orientation and multiple peaks with an intensity of 1.4 MRD were observed at the  $(2\bar{1}\bar{1}2)$  orientation and the corresponding symmetrically equivalent positions (Figure 3(c)). These peaks are not close to any of the symmetric tilt or twist orientations (see Figure 3(d)).

Figures 4 and 5 show grain boundary plane distributions at selected coincident site lattice (CSL) misorientations around the  $[10\bar{1}0]$  and  $[11\bar{2}0]$  axes. We have selected CSL (near CSL) boundaries separated by more than  $10^\circ$ , because this is the resolution of the distribution. For misorientations around the  $[0001]$  axes, the grain boundary plane distributions did not have maxima greater than 2 MRD and are not considered further. For the  $[10\bar{1}0]$  misorientation axis, there was a significant change in the grain boundary plane distribution with the misorientation angle (Figure 4). For the misorientation of  $10^\circ/[10\bar{1}0]$ , there were two peaks with an intensity of  $\sim 4$  MRD (Figure 4(a)). The first peak was located at the  $(10\bar{1}0)$  orientation, suggesting a twist character. There was also a high population for the orientations between the  $(10\bar{1}0)$  and  $(11\bar{2}0)$ . The second peak was positioned at the  $(01\bar{1}0)$  orientation, which was within the resolution of the distribution ( $4^\circ$ ) from the  $(0\ 7\ \bar{7}\ 1)$  twist boundary orientation (Figure 4(a,b)). At  $\sum 11 = 63^\circ/[10\bar{1}0]$ , multiple peaks appeared in the distribution (Figure 4(c)). The main peak was spread around the position of the  $(6\ \bar{3}\ \bar{3}\ 8)$  orientation with an intensity of 3.8 MRD (shown by the open circle in Figure 4(c)) and had a twist character (Figure 4(d)).

For the  $10^\circ/[11\bar{2}0]$  misorientation, the main peak had an intensity of only 2.75 MRD and broadly distributed around the  $(\bar{4}\ 5\ \bar{1}\ 1)$  orientation (shown by the open circle in Figure 5(a)), which was  $11^\circ$  from the  $(\bar{6}\ 6\ 0\ 1)$   $180^\circ$ -twist orientation (Figure 5(b)). A weaker peak was also present at the  $(0001)$  orientation (Figure 5(a)). At the  $\sum 23b = 34.3^\circ/[11\bar{2}0]$  misorientation, there was a relatively strong peak appeared at the  $(\bar{1}0\ 17\ \bar{7}\ 13)$  orientation with an intensity of 3.3 MRD (shown by the open circle in Figure 5(c)), which was  $11^\circ$  from the  $(\bar{8}\ 16\ \bar{8}\ 7)$  twist orientation (Figure 5(d)). At the  $\sum 9 = 56.3^\circ/[11\bar{2}0]$  misorientation, there was a peak at the  $(\bar{1}1\ 12\ \bar{1}\ 17)$  orientation with an intensity of 7.3 MRD (shown by an open circle in Figure 5(e)). This plane was  $10^\circ$  from the  $(\bar{1}101)$   $180^\circ$ -twist plane orientation (Figure 5(f)). For the  $\sum 15b = 86.2^\circ/[11\bar{2}0]$  misorientation, the main peak had an intensity of 7 MRD and an orientation of  $(2\bar{1}\bar{1}4)$  (shown by an open circle in Figure 5(g)). The peak was only  $8^\circ$  from the ideal  $(2\bar{1}\bar{1}3)$  twist position, which was less than the  $10^\circ$  resolution of the current measurement (Figure 5(h)). In all but one case, the peak in the distribution was within the experimental resolution of a geometrically special boundary.

The grain boundary plane distribution independent of misorientation is shown in Figure 6. It appeared that most boundaries were terminated on prismatic planes (i.e.  $\{hki0\}$ ), with a maximum value of 1.07 MRD at the  $(10\bar{1}0)$  orientation that spread towards  $(5\ \bar{2}\ \bar{3}\ 0)$  orientation. In other words, the population of these planes was 7% greater than expected in a random distribution. The minimum in distribution appeared at the  $(0001)$  basal plane orientation and had an intensity of 0.93 MRD (Figure 6).

The observations reported here reveal that the grain boundary plane distribution in this Mg alloy with a random texture is anisotropic. This is consistent

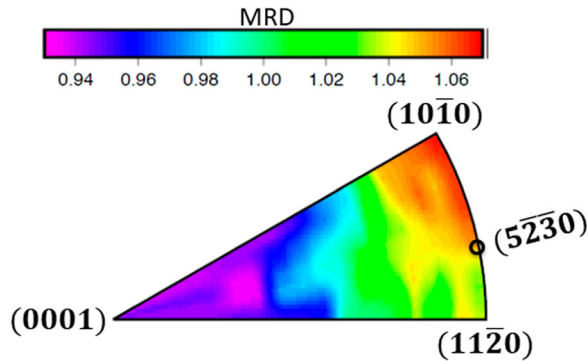


**Figure 6.** The grain boundary planes character distribution ignoring misorientation for AZ31 alloy with a random texture. MRD is multiples of random distribution. The reader is referred to the Web version of the article for the interpretation of colours in the figure (Colour online).

with the previous observations for different polycrystalline materials [7,8,10,11]. However, compared to other materials, the anisotropy in the Mg alloy studied is very weak. Assuming that this is not an artefact of the solidification and annealing, it suggests the grain boundary energy anisotropy is also relatively isotropic. Studies of a number of materials have concluded that the relative areas of grain boundaries are inversely correlated to the grain boundary energy for microstructures that result from normal grain growth [19]. In other words, the most frequently observed grain boundaries have the smallest energy and vice versa. This was demonstrated through various simulations [20–22] and experimental measurements [7,8,23,24]. The experiments were mostly carried out on polycrystalline materials with cubic structures, such as Ni [24], ferritic [7] and austenitic [8] steels.

In the absence of detailed knowledge of grain boundary energies, the interplanar spacing (i.e.  $d_{hkl}$ ) of the planes adjacent to a boundary can be used as a predictor of the relative grain boundary energy [25,26]. According to this model, boundaries composed of planes with large interplanar spacings have a relatively low energy. The rationale is that planes with large interplanar spacings are comparatively flat and smooth with fewer broken bonds and are likely to match better with the adjacent plane. Indeed, the attractive forces across the boundary are enhanced due to an improved fit at the interface, resulting in lower repulsion and a lower grain boundary energy [25,26]. In contrast, rougher planes, with smaller interplanar spacings, have more broken bonds and are less likely to

**Table 1.** The interplanar spacings ( $d_{hkl}$ ) for different planes observed in Figure 6.

Plane	Interplanar spacings (Å)
(10 $\bar{1}$ 0)	0.93 or 1.86 <sup>a</sup>
(11 $\bar{2}$ 0)	1.6
(5 $\bar{2}$ 30)	0.21 or 0.43 <sup>a</sup>
(0001)	2.6

<sup>a</sup>The structure factor was taken into account when the plane passing through an additional atom [27].

form a compact boundary structure with the adjacent plane. The interplanar spacings are summarised in Table 1 for planes that are labelled in Figure 6. Interestingly, there is no direct relationship between the populations and the interplanar spacing. In the distribution of grain boundary planes ignoring misorientation, the prismatic planes of  $(10\bar{1}0)$  and  $(5\bar{2}\bar{3}0)$  are the most frequent planes having  $1.86 \text{ \AA}$  (or  $0.93 \text{ \AA}$ ) and  $0.43 \text{ \AA}$  (or  $0.21 \text{ \AA}$ ) interplanar spacings, respectively (Table 1). However, the  $(0001)$  basal plane with the highest interplanar spacing of  $2.6 \text{ \AA}$  reveals the minimum population in the distribution (Figure 6, Table 1). In other words, assuming that the interplanar spacings are reliable predictors of the grain boundary energy, the planes with the maximum population have higher energy and vice versa.

Both the grain orientation texture (Figure 2(b)) and the grain boundary plane texture (Figure 6) are relatively random. Although there is some anisotropy in the grain boundary plane distribution, it is not strong. At specific misorientations, maxima in the distribution do not exceed 7 MRD and when misorientation is ignored, the deviation from random is only 7%. Interestingly, this weak anisotropy is similar to observations in another HCP metal,  $\alpha$ -Ti [28]. In cubic metals, these values are typically much larger. Although the casting was performed in the chill mould followed by prolonged annealing, there could be still a small amount of columnar (dendrite) grains remained from the as-cast microstructure in the final microstructure. It was shown that the growth direction of primary dendrite and its six secondary arms is along  $\langle 11\bar{2}0 \rangle$  direction in AZ91 Mg alloy [14]. Therefore, the lateral columnar surfaces should be at the orientations perpendicular to the  $\langle 11\bar{2}0 \rangle$  growth direction, including  $\{1\bar{1}00\}$  and  $(0001)$ . However, it appeared that these residual columnar grains largely contribute to the presence of prismatic planes (e.g.  $\{1\bar{1}00\}$ ) in the distribution rather  $(0001)$  (Figure 6). Therefore, the relative anisotropy observed in the grain boundary planes distribution is mostly related to the pre-existing columnar (dendrite) grains formed during solidification, which may remain after the prolonged annealing.

## Conclusions

The grain boundary plane distribution of an AZ31 Mg alloy with a random texture was studied using the five-parameter technique. The grain boundary plane distribution for different lattice misorientations associated with  $[10\bar{1}0]$  and  $[11\bar{2}0]$  misorientation axes displayed one or multiple peaks, which were usually close to a geometrically special boundary. The grain boundary plane distribution when misorientation is ignored showed relatively weak texture, which had a preference for prismatic  $\{hki0\}$  planes. Furthermore, the grain boundary plane distribution was not inversely correlated to the expected grain boundary energy. While the  $(0001)$  basal plane is assumed to have the smallest energy, it also has the minimum

population. This might be a result of the columnar grains, which was remained in the microstructure after prolonged annealing treatment.

## Acknowledgements

Deakin University's Advanced Characterisation Facility is acknowledged for use of the Quanta 3-D FEI scanning electron microscope.

## Disclosure statement

No potential conflict of interest was reported by the authors.

## Funding

The work at Deakin University was supported through grants provided by the Australian Research Council.

## References

- [1] M.H. Yoo, *Slip, twinning, and fracture in hexagonal close-packed metals*. Metall. Transact. A 12 (1981), pp. 409–418.
- [2] M.A. Meyers, O. Vohringer, and V.A. Lubarda, *The onset of twinning in metals: A constitutive description*. Acta Mater. 49 (2001), pp. 4025–4039.
- [3] L. Capolungo, P.E. Marshall, R.J. McCabe, I.J. Beyerlein, and C.N. Tome', *Nucleation and growth of twins in Zr: A statistical study*. Acta Mater. 57 (2009), pp. 6047–6056.
- [4] A. Ghaderi and M.R. Barnett, *Sensitivity of deformation twinning to grain size in titanium and magnesium*. Acta Mater. 59 (2011), pp. 7824–7839.
- [5] G.S. Rohrer, D.M. Saylor, B. El Dasher, B.L. Adams, A.D. Rollett, and P. Wynblatt, *The distribution of internal interfaces in polycrystals*. Z. Met.kd. 95 (2004), pp. 197–214.
- [6] H.H. Liu, S. Schmidt, H.F. Poulsen, A. Godfrey, Z.Q. Liu, J.A. Sharon, and X. Huang, *Three-dimensional orientation mapping in the transmission electron microscope*. Science 332 (2011), pp. 833–834.
- [7] H. Beladi and G.S. Rohrer, *The relative grain boundary area and energy distributions in a ferritic steel determined from three-dimensional electron backscatter diffraction maps*. Acta Mater. 61 (2013), pp. 1404–1412.
- [8] H. Beladi, N.T. Nuhfer, and G.S. Rohrer, *The five-parameter grain boundary character and energy distributions of a fully austenitic high-manganese steel using three dimensional data*. Acta Mater. 70 (2014), pp. 281–289.
- [9] D.M. Saylor, B.S. El-Dasher, B.L. Adams, and G.S. Rohrer, *Measuring the five-parameter grain-boundary distribution from observations of planar sections*. Metall. Mater. Transact. A 35 (2004), pp. 1981–1989.
- [10] D.M. Saylor, B. Dasher, Y. Pang, H.M. Miller, P. Wynblatt, A.D. Rollett, and G.S. Rohrer, *Habits of grains in dense polycrystalline solids*. J. Am. Ceram. Soc. 87 (2004), pp. 724–726.
- [11] H. Beladi and G.S. Rohrer, *The distribution of grain boundary planes in interstitial free steel*. Metall. Mater. Transact. A 44 (2013), pp. 115–124.

- [12] H. Beladi, G.S. Rohrer, A.D. Rollett, V. Tari, and P.D. Hodgson, *The distribution of intervariant crystallographic planes in a lath martensite using five macroscopic parameters*. Acta Mater. 63 (2014), pp. 86–98.
- [13] H. Beladi, Q. Chao, and G.S. Rohrer, *Variant selection and intervariant crystallographic planes distribution in martensite in a Ti-6Al-4V alloy*. Acta Mater. 80 (2014), pp. 478–489.
- [14] K. Pettersen and N. Ryum, *Crystallography of directionally solidified magnesium alloy AZ91*. Metall. Mater. Trans. A 20 (1989), pp. 847–852.
- [15] A. Serra, R.C. Pond, and D.J. Bacon, *Computer simulation of the structure and mobility of twinning dislocations in H.C.P. metals*. Acta Metall. et Mater 39 (1991), pp. 1469–1480.
- [16] K. Glowinski and A. Morawiec, *Twist, tilt, and symmetric grain boundaries in hexagonal materials*. J. Mater. Sci. 49 (2014), pp. 3936–3942.
- [17] A. Morawiec, *On interface-plane scheme and symmetric grain boundaries*. Z. Kristallogr 227 (2012), pp. 199–206.
- [18] M.R. Barnett, *Twinning and the ductility of magnesium alloys*. Mater. Sci. Eng. A 464 (2007), pp. 8–16.
- [19] G.S. Rohrer, *Grain boundary energy anisotropy: A review*. J. Mater. Sci. 46 (2011), pp. 5881–5895.
- [20] J. Gruber, D.C. George, A.P. Kuprat, G.S. Rohrer, and A.D. Rollett, *Effect of anisotropic grain boundary properties on grain boundary plane distributions during grain growth*. Scripta Mater 53 (2005), pp. 351–355.
- [21] G.S. Rohrer, J. Gruber, and A.D. Rollett, *A model for the origin of anisotropic grain boundary character distributions in polycrystalline materials*, in *Applications of Texture Analysis, in Ceramic Transactions of Applications of Texture Analysis*, A.D. Rollett, ed., John Wiley, Hoboken, NJ, 2009, Vol. 201, pp. 343–354.
- [22] J. Gruber, G.S. Rohrer, and A.D. Rollett, *Misorientation texture development during grain growth. Part II: Theory*. Acta Mater. 58 (2010), pp. 14–19.
- [23] S.J. Dillon and G.S. Rohrer, *Characterization of the grain boundary character and energy distributions of Yttria using automated serial sectioning and EBSD in the FIB*. J. Am. Ceram. Soc. 92 (2009), pp. 1580–1585.
- [24] J. Li, S.J. Dillon, and G.S. Rohrer, *Relative grain boundary area and energy distributions in nickel*. Acta Mater. 57 (2009), pp. 4304–4311.
- [25] D. Wolf, *Correlation between structure, energy, and ideal cleavage fracture for symmetrical grain boundaries in fcc metals*. J. Mater. Res. 5 (1990), pp. 1708–1730.
- [26] C.S. Kim and G.S. Rohrer, *Geometric and crystallographic characterization of WC surfaces and grain boundaries in WC-Co composites*. Interface Sci. 12 (2004), pp. 19–27.
- [27] Q. Fan, *A new method of calculating interplanar spacing: The position-factor method*. J. Appl. Crystall 45 (2012), pp. 1303–1308.
- [28] M.N. Kelly, K. Glowinski, N.T. Nuhfer, and G.S. Rohrer, *The five parameter grain boundary character distribution of  $\alpha$ -Ti determined from three-dimensional orientation data*. Acta Mater. 111 (2016), pp. 22–30.